ACS Photonics

Article

pubs.acs.org/journal/apchd5

Quantum Beats from Entangled Localized Surface Plasmons

Niket Thakkar,*[,†] Charles Cherqui,[‡] and David J. Masiello*[,†,‡]

[†]Department of Applied Mathematics and [‡]Department of Chemistry, University of Washington, Seattle, Washington 98195, United States

ABSTRACT: Recent experiments report observations of quantum interference between plasmon resonances, inviting descriptions of plasmon−photon interaction using methods from quantum optics. Here we demonstrate, using a Heisenberg−Langevin approach, that the radiation emitted from the localized surface plasmon resonances of a mixed-metal heterodimer may exhibit observable, beat frequency interferences at a far-field detector, known as quantum beats. This prediction represents a correspondence between **V**-type atoms of quantum optics and the familiar heterodimer system of plasmonics. We explore this analogy in depth and find that although both systems support quantum beats, the heterodimer emits photons in bunches due to the bosonic nature of the plasmon. This highlights a significant difference between the properties of atomic and plasmonic systems.

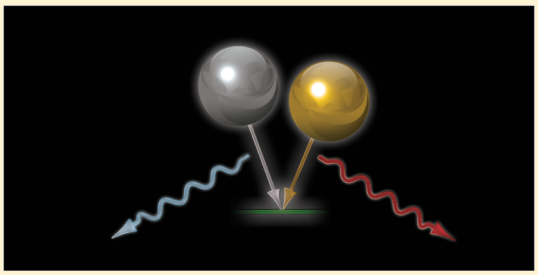

KEYWORDS: *quantum plasmonics, quantum beats, entangled plasmons, Fano interference*

The observation of Hong−Ou−Mandel (HOM) interference from propagating surface plasmons has established the close relationship between free-field photons and metal-confined surface plasmon polaritons.[1−4] In the original version of this experiment, single-photon interference at a 50−50 beam splitter induces fourth-order interference effects predicted by quantum electrodynamics.[5] The plasmonic HOM experiment reproduces this effect in the situation where interfering surface plasmons replace the beam splitter, opening the door for study of further parallels between plasmonics and quantum optics. Studies of the fundamental quantum-mechanical properties of plasma oscillations in conductors have allowed researchers to take advantage of the near-field properties of plasmonic structures in new ways. More specifically, recent experiments involving emission from quantum dots[6−8] or nitrogen-vacancy centers[9−12] coupled to metallic wave guides have shown the potential for plasmonic structures to be used as single-photon sources in quantum information science applications. Moreover, the plasmonic HOM experiment shows that quantum coherences are retained in photon−plasmon−photon conversion processes despite the significant dispersion and dephasing inherent to plasmonic systems.[1,2] The possibility of customizable, room-temperature quantum systems is significant for a variety of quantum information and computing applications, making quantum plasmonics an exciting and growing new field.[13,14]

The study of quantum interference between plasmons confined to the surfaces of metal nanoparticles has also generated significant recent research interest.[14−18] The optical properties of such localized surface plasmon resonances (LSPRs) have a rich dependence on particle morphology, material composition, and aggregation scheme, making LSPR systems highly tunable. In addition, aggregates of nanoparticles may support near-field regions of high electric field strength, so-called electromagnetic hot spots, which facilitate the manipulation of optical-frequency radiation at subdiffraction-limited length scales.[19−25] These features of LSPRs make them ideal candidates for a variety of applications requiring a high degree of optical control, and understanding their fundamental quantum-mechanical properties remains an important open question.

In this paper we study the radiation emitted from a simple LSPR system: two equal-sized silver and gold spheres in close proximity, supporting spectrally distinguishable dipole plasmon responses. Using a Heisenberg−Langevin approach, we model the interaction between the two spheres and the free-field, showing that the heterodimer has two radiative normal modes due to a Fano interference and generating a set of quantum Langevin equations that describe the evolution of the system. We then vary the system's initial Fock state and examine the observable differences in the far-field signal. We find that states with plasmons entangled between the heterodimer's two modes radiate with quantum beats, intensity fringes that oscillate with frequency equal to the difference between the fundamental frequencies of the two plasmon modes. This interference effect is the plasmonic analog of the quantum beats observed in so-called **V**-type atoms,[26] where two excited electronic states decay to the same ground state. However, although both the heterodimer and **V**-type atom support quantum beats, we find that, due to the bosonic nature of the LSPR, the two-photon statistics of radiation from each system are fundamentally different. While the **V**-type atom is known to emit antibunched light,[27] the plasmonic heterodimer emits photons that arrive at the detector in bunches.

Received: October 16, 2014
Published: December 21, 2014

DOI: 10.1021/ph500387c
ACS Photonics 2015, 2, 157−164

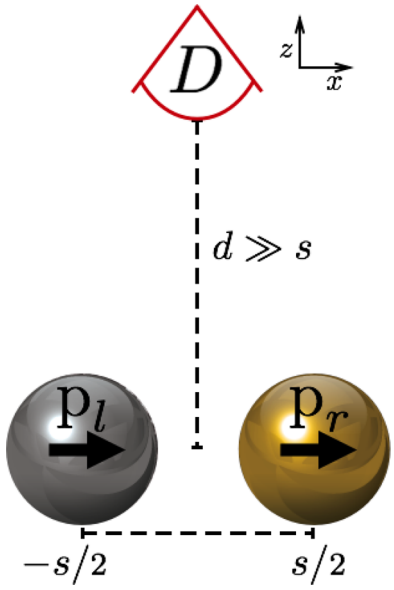

Figure 1. Heterodimer system composed of silver and gold nanospheres. We restrict our attention to each sphere's $\hat{x}$-polarized dipole plasmon, in aligned and antialigned configurations (the former is depicted). A far-field detector is placed along the z-axis equidistant from each sphere.

FANO INTERFERENCE IN THE HETERODIMER

We begin by building a description of two silver and gold spheres, both of radius a_0, coupled to a photon-field reservoir, as depicted in Figure 1. If we restrict our attention to the $\hat{\mathbf{x}}$-polarized, dipole plasmon on each sphere and neglect the zero-point energy, the Hamiltonian for this interacting plasmon-field system is

$$\begin{aligned}\hat{H} &= \hat{H}_{\mathrm{sys}} + \hat{H}_{\mathrm{res}} \\ &= \hbar\omega_l \hat{l}^\dagger \hat{l} + \hbar\omega_r \hat{r}^\dagger \hat{r} + \sum_{\mathbf{k}\lambda} \hbar\omega_{\mathbf{k}} \hat{f}^\dagger_{\mathbf{k}\lambda} \hat{f}_{\mathbf{k}\lambda} \\ &\quad + U(s)[\hat{l}^\dagger \hat{r} + \hat{r}^\dagger \hat{l}] + \sum_{\mathbf{k}\lambda} [\hbar g^l_{\mathbf{k}\lambda} \hat{f}^\dagger_{\mathbf{k}\lambda} \hat{l} + \hbar g^r_{\mathbf{k}\lambda} \hat{f}^\dagger_{\mathbf{k}\lambda} \hat{r}] + \text{h.c.}\end{aligned} \tag{1}$$

as derived in the Methods section. Here, the Hamiltonian is explicitly split into a coupled oscillator contribution for the plasmonic subsystem and an oscillator bath contribution for the free-photon reservoir. The plasmonic subsytem is described by the evolution of LSPR creation and annihilation operators $\hat{l}$, $\hat{l}^\dagger$ and $\hat{r}$, $\hat{r}^\dagger$ for the left and right spheres, respectively, and we assume without loss of generality that the silver sphere is on the left. The natural dipole plasmon frequencies for each sphere are ω_l and ω_r, and the two plasmons are coupled in the rotating-wave approximation with coupling constant $U(s) = 3\hbar(\omega_L\omega_R)^{1/2}a_0^3/s^3((\varepsilon^l_\infty + 2)(\varepsilon^r_\infty + 2))^{1/2}$, where $\varepsilon^{l,r}_\infty$ are the infinite frequency, static dielectric responses of silver and gold. Meanwhile, the reservoir contribution couples each plasmon to the free-field in the usual way,[27] where $\hat{f}_{\mathbf{k}\lambda}$ is the operator that annihilates a photon of wave vector $\mathbf{k}$ and polarization λ. The constants $\hbar g^l_{\mathbf{k}\lambda} = -\mathbf{p}_l \cdot \mathbf{E}_{\mathbf{k}\lambda}$ and $\hbar g^r_{\mathbf{k}\lambda} = -\mathbf{p}_r \cdot \mathbf{E}_{\mathbf{k}\lambda}$ couple the left- and right-localized plasmons to the photon electric field mode $\mathbf{E}_{\mathbf{k}\lambda} = (2\pi\hbar\omega_{\mathbf{k}}/V)^{1/2}\hat{\varepsilon}^\lambda_{\mathbf{k}} e^{i\mathbf{k}\cdot\mathbf{x}}$, where $\hat{\varepsilon}^\lambda_{\mathbf{k}}$ is a polarization vector and V is the quantization volume.

We note also the importance of choosing experimentally realizable parameters. For the remainder of the paper, we assume each sphere has a radius $a_0 = 25$ nm and is separated by a center−center distance $s = 60$ nm. The optical responses of both the silver and gold particles are described with a Drude model using plasma frequencies $\hbar\omega^l_p = 9.1$ eV and $\hbar\omega^r_p = 9.0$ eV, nonradiative dephasing rates of $\hbar\gamma_l = 0.05$ eV and $\hbar\gamma_r = 0.069$ eV, and infinite-frequency dielectric constants $\varepsilon^l_\infty = 3.77$ and $\varepsilon^r_\infty = 9.84$, respectively. Finally, these geometric and material parameter values are used in a discrete-dipole approximation-based simulation[28] to determine the spectral positions of the dipole resonances, $\hbar\omega_l = 3.6$ eV and $\hbar\omega_r = 2.6$ eV (see Figure 2), which are red-shifted slightly from the Clausius−Mossotti result due to relativistic effects. Given these parameters, all constants in the Hamiltonian can be easily calculated.

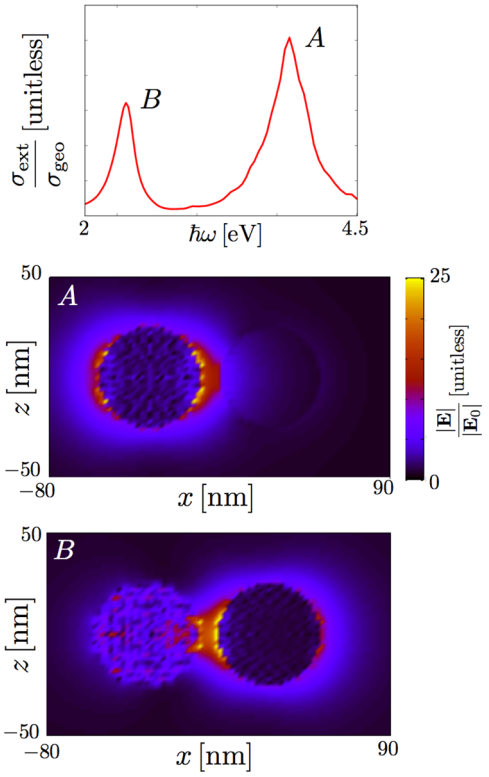

Figure 2. Full-wave simulation[28] of the heterodimer's extinction coefficient and electric near-field magnitude under plane-wave excitation. The extinction spectrum shows two peaks (labeled B and A) corresponding to the bonding and antibonding modes. Near-field plots of the target on resonance for each mode show that the modes are left and right localized, a consequence of a Fano interference, which allows both modes to radiate to the far-field. This localization effect is due to the heterogeneity in material composition of the target.

We proceed by diagonalizing the plasmonic subsystem contribution to the total Hamiltonian. To do so, we employ a canonical transformation with generating function $\hat{S} = i\theta(\hat{l}^\dagger \hat{r} - \hat{r}^\dagger \hat{l})$,[29] where we have defined the rotational angle

DOI: 10.1021/ph500387c
ACS Photonics 2015, 2, 157−164

$$\theta = \frac{1}{2}\arctan\left[\frac{2U(s)}{\hbar\omega_l - \hbar\omega_r}\right] \tag{2}$$

This diagonalization procedure gives rise to two uncoupled plasmon modes, $\hat{a} = \hat{l}\cos\theta - \hat{r}\sin\theta$ and $\hat{b} = \hat{r}\cos\theta + \hat{l}\sin\theta$. Expressing the Hamiltonian in this rotated basis gives

$$\hat{H} = \hbar\Omega_b\hat{b}^\dagger\hat{b} + \hbar\Omega_a\hat{a}^\dagger\hat{a} + \sum_{\mathbf{k}\lambda}\hbar\omega_{\mathbf{k}}\hat{f}^\dagger_{\mathbf{k}\lambda}\hat{f}_{\mathbf{k}\lambda} + \sum_{\mathbf{k}\lambda}[\hbar g^b_{\mathbf{k}\lambda}\hat{f}^\dagger_{\mathbf{k}\lambda}\hat{b} + \hbar g^a_{\mathbf{k}\lambda}\hat{f}^\dagger_{\mathbf{k}\lambda}\hat{a}] + \text{h.c.} \tag{3}$$

where $\hbar\Omega_a = \hbar\omega_l\cos^2\theta + \hbar\omega_r\sin^2\theta + 2U(s)\sin\theta\cos\theta$, $\hbar\Omega_b = \hbar\omega_r\cos^2\theta + \hbar\omega_l\sin^2\theta - 2U(s)\sin\theta\cos\theta$, $g^a_{\mathbf{k}\lambda} = g^l_{\mathbf{k}\lambda}\cos\theta - g^r_{\mathbf{k}\lambda}\sin\theta$, and $g^b_{\mathbf{k}\lambda} = g^r_{\mathbf{k}\lambda}\cos\theta + g^l_{\mathbf{k}\lambda}\sin\theta$. Here, $\Omega_{a,b}$ are the renormalized frequencies for the decoupled modes, and $\hbar g^{a,b}_{\mathbf{k}\lambda}$ are their renormalized coupling to the radiation field. This rotation casts $\hat{H}$ into the normal mode coordinates of the system, diagonalizing the plasmonic subsystem while maintaining coupling to the reservoir. The two normal modes correspond to the super- and subradiant modes predicted by hybridization models for coupled plasmonic systems.[30] To clarify the discussion and elucidate the analogy to coupled atom +field systems, we label the subradiant mode as a for antibonding and the super-radiant mode as b for bonding.

Interestingly, the rotation angle, θ (eq 2), is dependent on the ratio between the dipole coupling strength and the difference in resonant frequencies of the uncoupled LSPRs. For the physically realistic system under consideration the coupling is on the order of 10^{-2} eV and the detuning between the gold and silver particles is on the order of 1 eV, making the argument of the arctangent in eq 2 much smaller than unity. Within this parameter range, $\cos\theta \approx 1$ and $\sin\theta \approx 0$, making the bonding mode effectively right localized and the antibonding mode left localized. Furthermore, since each mode is the sum of two dipoles (i.e., $\mathbf{p}_a = \mathbf{p}_l\cos\theta - \mathbf{p}_r\sin\theta$ and $\mathbf{p}_b = \mathbf{p}_r\cos\theta + \mathbf{p}_l\sin\theta$), the localization of a plasmon on the left or right ensures that both modes couple to the electromagnetic field and therefore radiate. This is in contrast to the case of two spheres of identical size and composition: there the bonding mode would be "bright", while the antibonding mode would be "dark" since the latter would consist of two equal dipole plasmons oscillating out of phase and therefore have negligible total dipole moment. Thus, as a consequence of the asymmetry inherent in this mixed-material heterodimer, both modes can be observed with a far-field photon counter despite the electric dipole coupling, $U(s)$, allowing us to study far-field interference between the two modes. This asymmetry effect is often associated with a Fano resonance but can be expected from any coupled oscillator system with nondegenerate natural frequencies.[31] Its existence in heterodimer systems is verified experimentally in ref 32 and numerically in Figure 2.

As it must, the canonical transformation leaves commutation relations invariant, and the following Heisenberg equations of motion are readily obtained:

$$\begin{aligned} i\dot{\hat{a}} &= \Omega_a\hat{a} + \sum_{\mathbf{k}\lambda} g^{a*}_{\mathbf{k}\lambda}\hat{f}_{\mathbf{k}\lambda} \\ i\dot{\hat{b}} &= \Omega_b\hat{b} + \sum_{\mathbf{k}\lambda} g^{b*}_{\mathbf{k}\lambda}\hat{f}_{\mathbf{k}\lambda} \\ i\dot{\hat{f}}_{\mathbf{k}\lambda} &= \omega_{\mathbf{k}}\hat{f}_{\mathbf{k}\lambda} + g^a_{\mathbf{k}\lambda}\hat{a} + g^r_{\mathbf{k}\lambda}\hat{b} \end{aligned} \tag{4}$$

These are equivalent to the quantum master equations for the plasmonic subsystem and reservoir, since equations of motion for all observables are derivable from these results. Challenges arise from the last equation, which governs the dynamics of the infinite number of degrees of freedom in the reservoir. We handle this with the Heisenberg−Langevin approach, formally integrating the last equation and using the result to express the subsystem dynamics as an integral-differential equation dependent only on initial conditions and subsystem degrees of freedom.[27] Converting to slowly varying operators $\hat{A}(t) = \hat{a}\exp(i\Omega_a t)$ and $\hat{B}(t) = \hat{b}\exp(i\Omega_b t)$ yields modified equations of motion

$$\begin{aligned} \dot{\hat{A}}(t) &= \sum_{\mathbf{k}\lambda}[ig^{a*}_{\mathbf{k}\lambda}\hat{f}_{\mathbf{k}\lambda}(0)e^{-i(\Omega_a-\omega_{\mathbf{k}})t} \\ &\quad -|g^a_{\mathbf{k}\lambda}|^2\int_0^t dt'\hat{A}(t')e^{-i(\Omega_a-\omega_{\mathbf{k}})(t-t')} \\ &\quad -g^b_{\mathbf{k}\lambda}g^{a*}_{\mathbf{k}\lambda}\int_0^t dt'\hat{B}(t')e^{i\omega_{\mathbf{k}}(t-t')-i\Omega_a t+i\Omega_b t'}] \\ \dot{\hat{B}}(t) &= \sum_{\mathbf{k}\lambda}[ig^{b*}_{\mathbf{k}\lambda}\hat{f}_{\mathbf{k}\lambda}(0)e^{-i(\Omega_b-\omega_{\mathbf{k}})t} \\ &\quad -|g^b_{\mathbf{k}\lambda}|^2\int_0^t dt'\hat{B}(t')e^{-i(\Omega_b-\omega_{\mathbf{k}})(t-t')} \\ &\quad -g^a_{\mathbf{k}\lambda}g^{b*}_{\mathbf{k}\lambda}\int_0^t dt'\hat{A}(t')e^{i\omega_{\mathbf{k}}(t-t')-i\Omega_b t+i\Omega_a t'}] \end{aligned} \tag{5}$$

In both equations the final term corresponds to a multiple scattering event. Such terms will be neglected since we assume that the spheres do not interact through the reservoir, an assumption that is equivalent to the Markov approximation.[33] The remaining integral is calculated in the Weisskopf−Wigner approximation,[27,33] and we find

$$\begin{aligned} \dot{\hat{A}}(t) &= -\frac{C_a+\gamma_a}{2}\hat{A}(t) + \hat{F}_a(t) \\ \dot{\hat{B}}(t) &= -\frac{C_b+\gamma_b}{2}\hat{B}(t) + \hat{F}_b(t) \end{aligned} \tag{6}$$

Here $C_a = 4\Omega_a^3|\mathbf{p}_a|^2/3\hbar c^3$, $C_b = 4\Omega_b^3|\mathbf{p}_b|^2/3\hbar c^3$, $\gamma_a = \gamma_l\cos^2\theta + \gamma_r\sin^2\theta$, $\gamma_b = \gamma_r\cos^2\theta + \gamma_l\sin^2\theta$, and

$$\begin{aligned} -i\hat{F}_a(t) &= \sum_{\mathbf{k}\lambda} g^{a*}_{\mathbf{k}\lambda}\hat{f}_{\mathbf{k}\lambda}(0)e^{-i(\Omega_A-\omega_{\mathbf{k}})t} \\ -i\hat{F}_b(t) &= \sum_{\mathbf{k}\lambda} g^{b*}_{\mathbf{k}\lambda}\hat{f}_{\mathbf{k}\lambda}(0)e^{-i(\Omega_B-\omega_{\mathbf{k}})t} \end{aligned} \tag{7}$$

are known as noise operators. The equations of motion above are so-called quantum Langevin equations, since the operators $\hat{F}_a$ and $\hat{F}_b$ model stochastic forcing due to the system−reservoir interaction. Unlike the classical case, here the stochastic forcing is a quantum-mechanical operator that can be handled at the level of ensemble averages. These averages depend on the initial

DOI: 10.1021/ph500387c
ACS Photonics 2015, 2, 157−164

state of the reservoir, which in our case is assumed to be evacuated. Interaction with the reservoir also gives rise to dissipation at rates C_a and C_b in accordance with the fluctuation−dissipation theorem. Note that we also incorporate nonradiative damping at this level by adding the aforementioned dephasing rates, γ_a and γ_b, to the radiative damping term.

We complete our description by discussing the far-field photon counter, a quantum-mechanical instrument that can be modeled with Glauber correlation functions.[34] Of interest are two observables in particular, the normalized intensity,

$$I(t) = \frac{\langle \hat{\mathbf{E}}^-(t)\, \hat{\mathbf{E}}^+(t)\rangle}{\langle \hat{\mathbf{E}}^-(0)\, \hat{\mathbf{E}}^+(0)\rangle} \tag{8}$$

and the normalized, second-order correlation

$$g^{(2)}(\tau) = \frac{\langle \hat{\mathbf{E}}^-(0)\, \hat{\mathbf{E}}^-(\tau)\, \hat{\mathbf{E}}^+(\tau)\, \hat{\mathbf{E}}^+(0)\rangle}{|\langle \hat{\mathbf{E}}^-(0)\, \hat{\mathbf{E}}^+(0)\rangle|^2} \tag{9}$$

both assumed to be evaluated at the location of the detector, $\mathbf{r} = d\hat{\mathbf{z}}$, with expectation values taken with respect to a particular Fock state for the system. Here, $\hat{\mathbf{E}}^{\pm}(t)$ are the positive and negative frequency components of the total field operator. $I(t)$ is a measure of the relative probability that a photon arrives at the detector at time t, while $g^{(2)}(\tau)$ is a measure of the relative probability that two photons arrive separated by a delay time τ (the first photon is assumed to arrive at $t = 0$). Known as the second-order correlation, $g^{(2)}(\tau)$ probes for the existence of higher-order interference effects like those observed in the HOM experiment.[5] For the system under consideration, the field operators can be written in terms of plasmonic subsystem degrees of freedom using the equations of motion.[27] We find

$$\hat{\mathbf{E}}^+(\mathbf{x}, t) = \hat{\mathbf{x}}\frac{\Omega_a^2 p_a}{c^2|\mathbf{x}-\mathbf{r}_l|}\left[e^{-i\Omega_a\left(t-\frac{|\mathbf{x}-\mathbf{r}_l|}{c}\right)}\hat{A}\left(t-\frac{|\mathbf{x}-\mathbf{r}_l|}{c}\right)\right] + \hat{\mathbf{x}}\frac{\Omega_b^2 p_b}{c^2|\mathbf{x}-\mathbf{r}_r|}\left[e^{-i\Omega_b\left(t-\frac{|\mathbf{x}-\mathbf{r}_r|}{c}\right)}\hat{B}\left(t-\frac{|\mathbf{x}-\mathbf{r}_r|}{c}\right)\right] \tag{10}$$

where $\mathbf{r}_l = -s/2\hat{x}$ and $\mathbf{r}_r = s/2\hat{x}$. This implies that calculating the time-dependent expectation values of all normal ordered, number-conserving combinations of two or four subsystem operators A and B fully specifies the expectation values in eq 8 and eq 9. This calculation may be performed by constructing and solving equations of motion for the operators using eq 6 with knowledge of the evacuated initial state of the reservoir.

PLASMONIC INTERFERENCE EFFECTS AND DISCUSSION

Single-Photon Dynamics and Quantum Beats. We turn to modeling radiation emitted from the plasmonic heterodimer and search for far-field signals of entanglement by comparing the decay of two fundamentally different LSPR Fock states,

$$|\psi_S\rangle = |1_a 0_b\rangle$$
$$|\psi_E\rangle = \frac{|1_a 0_b\rangle + |0_a 1_b\rangle}{\sqrt{2}} \tag{11}$$

where a single Fock state, $|n_a, m_b\rangle$, is specified by occupation numbers n and m for the decoupled sub- and super-radiant modes; the former is the antibonding mode, while the latter is the bonding mode. The state $|\psi_S\rangle$ is a single LSPR Fock state, where we assume that a photon of frequency Ω_a is used to excite a plasmon in the left-localized mode. Exciting a single plasmon state is nontrivial, but experimentalists have succeeded in doing so in related systems by coupling to quantum emitters that saturate (e.g., quantum dots[8] or nitrogen-vacancy centers[12]) or potentially with an electron beam in an electron energy-loss spectroscopy experiment.[35−37] It is interesting to note that, although $|\psi_S\rangle$ must be excited by a single photon, its normalized intensity is indistinguishable from an LSPR excited by classical light (i.e., a coherent LSPR state, $|\beta_a 0_b\rangle = e^{-|\beta|^2/2}\sum_{n=0}^{\infty}\beta^n|n_a 0_b\rangle/\sqrt{n!}$, with arbitrary average occupation number $|\beta|^2$). This state, $|\psi_S\rangle$, is contrasted with $|\psi_E\rangle$, an entangled LSPR Fock state generated by a single pump photon entangled between both modes. Such a photon exhibits similar entanglement properties to those generated via spontaneous parametric down-conversion[38] in both the optical and plasmonic HOM experiments,[1,2,5] and we show here that the radiative decay of the plasmonic state with nontrivial quantum coherences gives rise to an observably different far-field signal than its nonentangled counterpart, $|\psi_S\rangle$.

The transient intensity signal observed at the detector displayed in Figure 4 is computed from the Heisenberg−

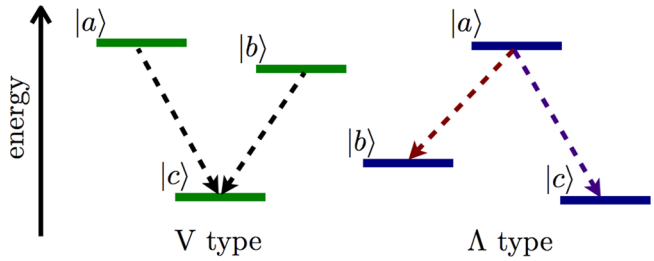

Figure 3. **V**- and **Λ**-type systems are descriptions used in quantum optics of certain electronic state configurations within atoms. In the **V** system, two excited states may transition to the same ground state, making one transition indistinguishable from the other. On the other hand, in the **Λ** system, a single excited state transitions to one of two distinguishable ground states. Classical electrodynamics predicts that both systems will have interference effects, but quantum electrodynamics does not. Instead, since only the **V** system has indistinguishable pathways, it is the only system that exhibits interferences, known as quantum beats.[27,33]

Langevin approach described in the previous section. While the expected intensity for the single LSPR Fock state is monotonically decreasing because the plasmon decays along a single channel, the entangled state exhibits interference between the possibilities for the plasmon to decay along the super- or subradiant modes, giving rise to oscillations at the system's beat frequency, $\Omega_a - \Omega_b$. For this system in particular, the beat frequency is approximately 1 eV/$\hbar$, implying that the effect takes place well within the observed lifetime of the plasmon (on the order of 10 fs). Thus, we expect these interference fringes to be observable with state-of-the-art photon counters.[39]

If experimentally verified, plasmonic quantum beats offer further proof of the close connection between LSPRs and free-field photons. As a consequence, we see that nanoparticle aggregates with multiple, noninteracting "bright" modes, as is the case in plasmonic Fano resonance supporting systems, have quantum-mechanical descriptions that are equivalent to those for optical interferometers. For the heterodimer system discussed in this paper, the super- and subradiant modes each

DOI: 10.1021/ph500387c
ACS Photonics 2015, 2, 157−164

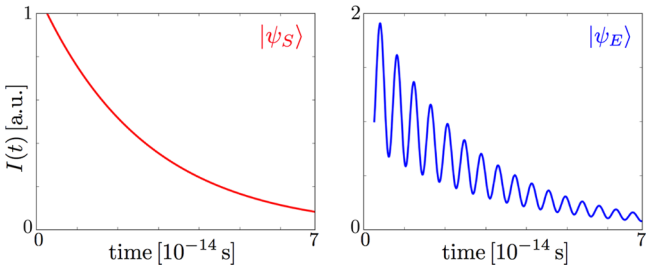

Figure 4. We compare the dynamics of the expected intensity signal from a single LSPR Fock state, $|\psi_S\rangle$, and a superposition LSPR state, $|\psi_E\rangle$, excited by an entangled photon. In the former case, the signal decreases monotonically over time, while, in the latter case, the signal exhibits oscillations at the beat frequency of the heterodimer system. This is due to the fact that $|\psi_S\rangle$ decays only through the antibonding mode, while $|\psi_E\rangle$ may decay through both bonding and antibonding modes, leading to an interference in the intensity signal. These interference-induced oscillations, known as quantum beats, serve as an observable, far-field signature of an entangled LSPR Fock state in the single-plasmon limit. Note that, in both cases, the signal starts at a nonzero time due to the travel time of photons from the heterodimer to the detector.

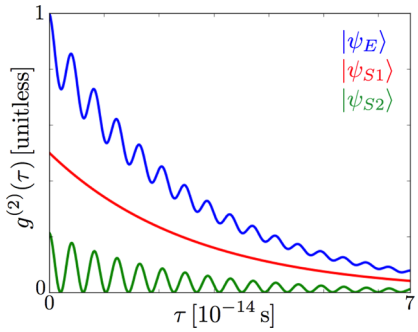

Figure 5. We compare the normalized, second-order photon correlation expected from three different LSPR Fock states. $|\psi_{S1}\rangle$ corresponds to a two-photon pumping of just the left-localized mode, $|\psi_{S2}\rangle$ corresponds to exciting each mode individually, and $|\psi_E\rangle$ is an excited state where two plasmons are entangled between the left- and right-localized modes. All three states exhibit varying degrees of photon bunching, but the degree of correlation varies from state to state.

decay to the vacuum in direct correspondence with atomic systems having two excited electronic states transitioning to the same ground state. These so-called **V**-type atoms, in contrast to **Λ**-type atoms (where an excited state can transition to two distinct lower energy states), are known to exhibit observable quantum beats as a result of the interference between possibilities for energy to come from one of two indistinguishable transitions (see Figure 3).[33] For the one-photon dynamics, the situation is no different for the heterodimer, and these plasmonic quantum beats therefore provide an observable signature of an entangled LSPR Fock state in the single-plasmon limit. Moreover, this interferometer description of noninteracting, radiating modes is a useful way to interpret the dynamics of more complicated nanoparticle aggregates.

Two-Photon Dynamics and Photon Bunching. The plasmonic heterodimer and the **V**-type atom behave similarly only in the one-photon case. The statistical correlation between two photons emitted by the heterodimer sets it apart from the atomic analog. To see this, we compare the states

$$|\psi_{S1}\rangle = |2_a 0_b\rangle$$
$$|\psi_{S2}\rangle = |1_a 1_b\rangle$$
$$|\psi_E\rangle = \frac{|2_a 0_b\rangle + |0_a 2_b\rangle}{\sqrt{2}} \quad (12)$$

Here, the first two states result from pumping with nonentangled light, while the last state is assumed to be excited by entangled photons just as in the previous section. The LSPR Fock state $|\psi_{S1}\rangle$ models a typical pumping of just the left-localized mode, while $|\psi_{S2}\rangle$ models an excitation where both the super- and subradiant modes are pumped with one photon individually.

Normalized, second-order correlations, $g^{(2)}(\tau)$, for each LSPR Fock state are plotted in Figure 5. These are calculated with the Heisenberg–Langevin approach described previously under the assumption that the emitted field is time-translation invariant. Interestingly, we see a higher probability for short delay times in all three cases, indicating varying degrees of photon bunching for all three LSPR Fock states. This interference effect is a direct result of the bosonic nature of the plasmon–photon system. More explicitly, photon detection at $t = 0$ and at $t = \tau$ occurs in six different ways: (1) two photons can be emitted due to decay along mode A at $t = -|\mathbf{r} - \mathbf{r}_l|/c$ and $t = \tau - |\mathbf{r} - \mathbf{r}_l|/c$, (2) two photons can be emitted due to decay along mode B at $t = -|\mathbf{r} - \mathbf{r}_r|/c$ and $t = \tau - |\mathbf{r} - \mathbf{r}_r|/c$, (3) mode A can decay at $t = -|\mathbf{r} - \mathbf{r}_l|/c$ and mode B at $t = \tau - |\mathbf{r} - \mathbf{r}_r|/c$, and (4–6) all three previous possibilities can happen in reverse order. These channels are depicted in Figure 6. Since

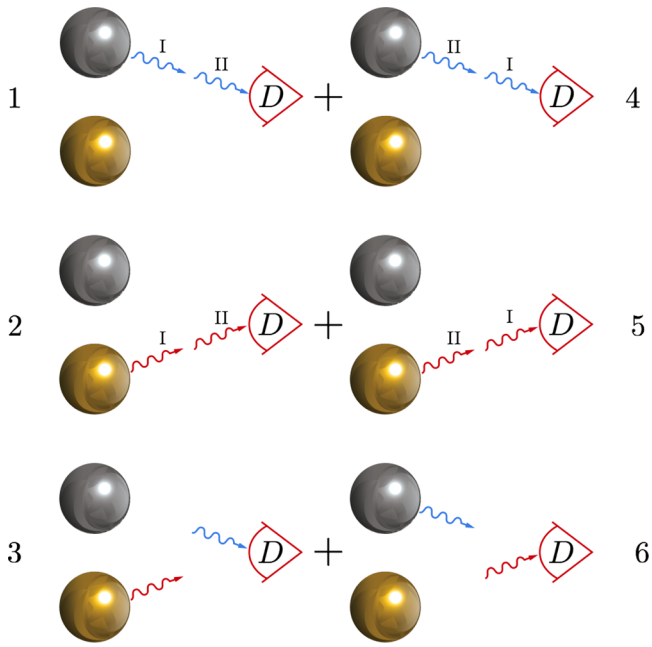

Figure 6. Photon detection in the far-field at time $t = 0$ and $t = \tau$ can occur in six different ways for the heterodimer considered in this paper. On the left-hand side, the possibilities that two photons come from A, two photons come from B, and one photon comes from each are depicted (note that the Roman numerals serve to distinguish what otherwise should be indistinguishable photons). Meanwhile, on the right-hand side, the two photons on the left are exchanged, allowing for three more possibilities. The channels on the right interfere constructively with the channels on the left due to the bosonic nature of the plasmon–photon system.

DOI: 10.1021/ph500387c
ACS Photonics 2015, 2, 157–164

the system's wave function is symmetric under boson exchange, each possibility will interfere constructively with its reverse process for delay times within the lifetime of the plasmon, and thus all three states exhibit some degree of bunching. However, only $|\psi_E\rangle$ has access to interference from all six possibilities, accounting for the anomalously high degree of correlation exhibited by the entangled state. Meanwhile, oscillations in two of the signals arise from the phase difference between photons emitted from the left- and right-localized modes, explaining why the signal from the entirely left-localized LSPR Fock state is free of oscillations. This reasoning was first presented for a more general system by Fano, and mathematical details can be found in his paper.[40]

Photon bunching in LSPR systems allows us to draw comparisons to the plasmonic HOM experiment, which measures coincidence counts, the all-time integral of the second-order correlation.[5] In that case, the emitted photons exhibit bunching at one detector or another for short delay times as a result of purely quantum-mechanical interference between two propagating plasmons.[1,2] Although we expect photons emitted from LSPR systems to be bunched as well, the effect takes place for fundamentally different physical reasons. For our purposes, we see clearly from Figure 5 that an anomalously high degree of bunching is another far-field signature of an entangled LSPR Fock state. Moreover, the reasoning above is one that can be applied in general to systems of interacting bosons, which, interestingly, indicates that radiation from more complicated nanoparticle aggregates should always be bunched, regardless of the details of the LSPR Fock state decaying to the far-field.

This result breaks the analogy between the plasmonic heterodimer and **V**-type atoms. In the atomic system, the radiating dipole is created by an oscillating electron, a system that must exhibit Fermion statistics. In fact, radiation from **V**-type atoms is known to be antibunched; that is, two photons have a *low* probability of arriving with a short delay time τ.[27] Physically, this occurs because the electron must relax to a ground state when it emits and then must be excited again before emitting a second photon, in contrast to the plasmon, which can be pumped with multiple photons at once. This, fundamentally, is the difference between a Fermionic and bosonic oscillator, and it is this difference that gives rise to differences in two-photon interferences from each of the two systems.

CONCLUSION

Using a Heisenberg–Langevin approach we have modeled the quantum-mechanical properties of the optical-frequency electromagnetic radiation emitted from the hybridized localized surface plasmons of a mixed-metal heterodimer. A canonical transformation was used to diagonalize the plasmonic contributions to the Hamiltonian, showing simply that the heterodimer system supports sub- and super-radiant normal modes that remain coupled to the free-field. We have predicted that plasmon entanglement across these heterodimer modes is observable in the far-field, despite the inherent radiative and nonradiative damping associated with LSPRs. Because the entangled LSPR Fock state can decay along two indistinguishable pathways, its emitted radiation exhibits interferences at the system's beat frequency, so-called quantum beats. This effect parallels the quantum beats observed in the radiation emitted from certain electronic transitions in **V**-type atoms (see Figure 3), a parallel that offers a qualitative way to interpret the single-photon dynamics of more complicated nanoparticle aggregates. We show further that the analogy between plasmon–photon and atom–photon interaction only goes so far. In fact, emitted photons from the heterodimer are positively correlated and can be expected to arrive at the detector in bunches. On the other hand, the opposite has been observed for **V**-type atoms.[27] The difference in photon correlation can be attributed to the difference in quantum statistics of the two emitters. This breakdown of the analogy between plasmonic and atomic systems is true in general and applies to interpretations of the physics of more complicated LSPR-supporting nanoparticle aggregates.

METHODS

Derivation of the Quantum Plasmon Hamiltonian. The oscillator Hamiltonian in eq 1 can be derived by first approximating the electric polarization induced in each sphere as an LSPR oscillator with dipole moment **p**. This approach was developed first by Lucas and co-workers[41] for the case of classical coupled LSPRs, while the quantization of a single nanosphere's plasmon modes was first developed by Ritchie and co-workers.[42,43] These approaches are applied in detail in a variety of references; see, for example, refs 19 and 44. Here, we begin with the result

$$H_0 = \frac{\boldsymbol{\mathcal{P}}_l^2}{2m_l} + \frac{1}{2}m_l\omega_l^2\mathbf{u}_l^2 + \frac{\boldsymbol{\mathcal{P}}_r^2}{2m_r} + \frac{1}{2}m_r\omega_r^2\mathbf{u}_r^2 + V_{\text{int}} \tag{13}$$

where $\mathbf{u}_{l,r} = \mathbf{p}_{l,r}/(-e)$ are generalized coordinates with conjugate momenta $\boldsymbol{\mathcal{P}}_{l,r}$, $\omega_{l,r}$ are the dipole plasmon frequencies for the left and right spheres, and $m_{l,r} = e^2/\alpha_{l,r}\omega_{l,r}^2$ are the oscillator masses defined in terms of the surface plasmon polarizabilities for each sphere, $\alpha_{l,r} = 3a_0^3/(\varepsilon_\infty^{l,r} + 2)$ in the Drude approximation to the metal's dielectric response.

The mutual electric dipole–dipole interaction, $V_{\text{int}} = -\mathbf{p}_l\cdot\boldsymbol{\Lambda}^0\cdot\mathbf{p}_r$, takes the form

$$V_{\text{int}} = \frac{e^2}{s^3}\mathbf{u}_l\cdot[3\hat{\mathbf{n}}_{lr}\hat{\mathbf{n}}_{lr} - 1]\cdot\mathbf{u}_r \tag{14}$$

where $\hat{\mathbf{n}}_{lr}$ is the unit vector between the left and right dipole, and we restrict ourselves to the near-field component $\boldsymbol{\Lambda}^0$ of the dipole relay tensor. Finally, further restricting ourselves to *x*-polarized dipoles, quantizing the harmonic oscillators in the standard way, and making the rotating wave approximation, we have

$$\hat{H}_{\text{sys}} = \hbar\omega_l\hat{l}^\dagger\hat{l} + \hbar\omega_r\hat{r}^\dagger\hat{r} + U(s)[\hat{l}^\dagger\hat{r} + \hat{r}^\dagger\hat{l}] \tag{15}$$

Here, $\hat{l}(\hat{l}^\dagger)$ and $\hat{r}(\hat{r}^\dagger)$ are the annihilation (creation) operators for plasmons on the left and right sphere, respectively, defined in terms of the original coordinates as

$$l = \sqrt{\frac{m_l\omega_l}{2\hbar}}\left(\mathbf{u}_l + \frac{i}{m_l\omega_l}\boldsymbol{\mathcal{P}}_l\right)\cdot\hat{\mathbf{x}} \rightarrow \hat{l}$$

$$r = \sqrt{\frac{m_r\omega_r}{2\hbar}}\left(\mathbf{u}_r + \frac{i}{m_r\omega_r}\boldsymbol{\mathcal{P}}_r\right)\cdot\hat{\mathbf{x}} \rightarrow \hat{r}, \tag{16}$$

with the dagger operators obtained by Hermitian conjugate. Meanwhile, the interaction energy between the dipoles reduces to $U(s) = 3\hbar(\omega_L\omega_R)^{1/2}a_0^3/s^3((\varepsilon_\infty^l + 2)(\varepsilon_\infty^r + 2))^{1/2}$.

We complete the derivation of the Hamiltonian by including the energetic contribution of the free-photon field. This is done

DOI: 10.1021/ph500387c
ACS Photonics 2015, 2, 157–164

in the standard way, where modes of the electric field with polarization λ and wave vector $\mathbf{k}$ and $\mathbf{E}_{\mathbf{k}\lambda}$ are treated as an infinite set of uncoupled, quantum oscillators and each plasmon dipole couples to each electric field mode with interaction energy $\hbar g_{\mathbf{k}\lambda}^{l,r} = -\mathbf{p}_{l,r}\cdot\mathbf{E}_{\mathbf{k}\lambda}$.[27,33] The combination of system and reservoir degrees of freedom yields the Hamiltonian $\hat{H}$ used in this paper.

AUTHOR INFORMATION

Corresponding Authors

*E-mail: thakkar@u.washington.edu.

*E-mail: masiello@chem.washington.edu.

Notes

The authors declare no competing financial interest.

ACKNOWLEDGMENTS

This work was supported by the National Science Foundation's CAREER program under award number CHE-1253775 (D.J.M.), NSF XSEDE resources under award number PHY-130045 (D.J.M.), and the NSF Graduate Research Fellowship Program under award number DGE-1256082 (N.T.). The authors would also like to thank Prof. Arka Majumdar of the University of Washington and Dr. Robert L. Cook of the University of New Mexico for helpful discussions, as well as Nipa Eason (http://nipaeason.com) for graphic design contributions to this work.

REFERENCES

(1) Fakonas, J. S.; Lee, H.; Kelaita, Y. A.; Atwater, H. A. Two-plasmon quantum interference. *Nat. Photonics* **2014**, *8*, 317−320.

(2) Fujii, G.; Fukuda, D.; Inoue, S. Direct observation of bosonic quantum interference of surface plasmon polaritons using photon-number-resolving detectors. *Phys. Rev. B* **2014**, *90*, 085430.

(3) Di Martino, G.; Sonnefraud, Y.; Tame, M.; Kéna-Cohen, S.; Dieleman, F.; Özdemir, S.; Kim, M.; Maier, S. Observation of quantum interference in the plasmonic Hong-Ou-Mandel effect. *Phys. Rev. Appl.* **2014**, *1*, 034004.

(4) Cai, Y.-J.; Li, M.; Ren, X.-F.; Zou, C.-L.; Xiong, X.; Lei, H.-L.; Liu, B.-H.; Guo, G.-P.; Guo, G.-C. High-visibility on-chip quantum interference of single surface plasmons. *Phys. Rev. Appl.* **2014**, *2*, 014004.

(5) Hong, C.; Ou, Z.; Mandel, L. Measurement of subpicosecond time intervals between two photons by interference. *Phys. Rev. Lett.* **1987**, *59*, 2044.

(6) Falk, A. L.; Koppens, F. H.; Chun, L. Y.; Kang, K.; de Leon Snapp, N.; Akimov, A. V.; Jo, M.-H.; Lukin, M. D.; Park, H. Near-field electrical detection of optical plasmons and single-plasmon sources. *Nat. Phys.* **2009**, *5*, 475−479.

(7) de Leon, N. P.; Shields, B. J.; Chun, L. Y.; Englund, D. E.; Akimov, A. V.; Lukin, M. D.; Park, H. Tailoring light-matter interaction with a nanoscale plasmon resonator. *Phys. Rev. Lett.* **2012**, *108*, 226803.

(8) Akimov, A.; Mukherjee, A.; Yu, C.; Chang, D.; Zibrov, A.; Hemmer, P.; Park, H.; Lukin, M. Generation of single optical plasmons in metallic nanowires coupled to quantum dots. *Nature* **2007**, *450*, 402−406.

(9) Huck, A.; Kumar, S.; Shakoor, A.; Andersen, U. L. Controlled coupling of a single nitrogen-vacancy center to a silver nanowire. *Phys. Rev. Lett.* **2011**, *106*, 096801.

(10) Kolesov, R.; Grotz, B.; Balasubramanian, G.; Stöhr, R. J.; Nicolet, A. A.; Hemmer, P. R.; Jelezko, F.; Wrachtrup, J. Wave−particle duality of single surface plasmon polaritons. *Nat. Phys.* **2009**, *5*, 470−474.

(11) Fedutik, Y.; Temnov, V.; Schöps, O.; Woggon, U.; Artemyev, M. Exciton-plasmon-photon conversion in plasmonic nanostructures. *Phys. Rev. Lett.* **2007**, *99*, 136802.

(12) Cuche, A.; Mollet, O.; Drezet, A.; Huant, S. Deterministic quantum plasmonics. *Nano Lett.* **2010**, *10*, 4566−4570 PMID: 20964345.

(13) Tame, M.; McEnery, K.; Özdemir, Ş.; Lee, J.; Maier, S.; Kim, M. Quantum plasmonics. *Nat. Phys.* **2013**, *9*, 329−340.

(14) del Pino, J.; Feist, J.; Garca-Vidal, F.; Garca-Ripoll, J. J. Entanglement detection in coupled particle plasmons. *Phys. Rev. Lett.* **2014**, *112*, 216805.

(15) Lee, C.; Tame, M.; Lim, J.; Lee, J. Quantum plasmonics with a metal nanoparticle array. *Phys. Rev. A* **2012**, *85*, 063823.

(16) Frank, R. Coherent control of Floquet-mode dressed plasmon polaritons. *Phys. Rev. B* **2012**, *85*, 195463.

(17) Lawrie, B.; Evans, P.; Pooser, R. Extraordinary optical transmission of multimode quantum correlations via localized surface plasmons. *Phys. Rev. Lett.* **2013**, *110*, 156802.

(18) Lee, C.; Tame, M.; Noh, C.; Lim, J.; Maier, S. A.; Lee, J.; Angelakis, D. G. Robust-to-loss entanglement generation using a quantum plasmonic nanoparticle array. *New J. Phys.* **2013**, *15*, 083017.

(19) Cherqui, C.; Bigelow, N. W.; Vaschillo, A.; Goldwyn, H.; Masiello, D. J. Combined tight-binding and numerical electrodynamics understanding of the STEM/EELS magneto-optical responses of aromatic plasmon-supporting metal oligomers. *ACS Photonics* **2014**, *1*, 1013−1024.

(20) Sönnichsen, C.; Franzl, T.; Wilk, T.; von Plessen, G.; Feldmann, J.; Wilson, O.; Mulvaney, P. Drastic reduction of plasmon damping in gold nanorods. *Phys. Rev. Lett.* **2002**, *88*, 077402.

(21) Maier, S. A. Localized surface plasmons. *Plasmonics: Fundam. Appl.* **2007**, 65−88.

(22) Stockman, M. I. Nanoplasmonics: past, present, and glimpse into future. *Opt. Express* **2011**, *19*, 22029−22106.

(23) Jensen, T. R.; Malinsky, M. D.; Haynes, C. L.; Van Duyne, R. P. Nanosphere lithography: tunable localized surface plasmon resonance spectra of silver nanoparticles. *J. Phys. Chem. B* **2000**, *104*, 10549−10556.

(24) Nordlander, P.; Oubre, C.; Prodan, E.; Li, K.; Stockman, M. Plasmon hybridization in nanoparticle dimers. *Nano Lett.* **2004**, *4*, 899−903.

(25) Kirakosyan, A.; Stockman, M.; Shahbazyan, T. *Surface plasmon lifetime in metal nanoshells*. arXiv preprint *arXiv:0908.0647*, 2009.

(26) Forrester, A. T.; Gudmundsen, R. A.; Johnson, P. O. Photoelectric mixing of incoherent light. *Phys. Rev.* **1955**, *99*, 1691.

(27) Scully, M. O. *Quantum Optics*; Cambridge University Press, 1997.

(28) Draine, B. T.; Flatau, P. J. Discrete-dipole approximation for scattering calculations. *J. Opt. Soc. Am. A* **1994**, *11*, 1491−1499.

(29) Wagner, M. *Unitary Transformations in Solid State Physics*; Elsevier Science Publishers, 1986.

(30) Nordlander, P.; Oubre, C.; Prodan, E.; Li, K.; Stockman, M. I. Plasmon hybridization in nanoparticle dimers. *Nano Lett.* **2004**, *4*, 899−903.

(31) Joe, Y. S.; Satanin, A. M.; Kim, C. S. Classical analogy of Fano resonances. *Phys. Scr.* **2006**, *74*, 259.

(32) Brown, L. V.; Sobhani, H.; Lassiter, J. B.; Nordlander, P.; Halas, N. J. Heterodimers: plasmonic properties of mismatched nanoparticle pairs. *ACS Nano* **2010**, *4*, 819−832.

(33) Meystre, P.; Sargent, M. *Elements of Quantum Optics*; Springer, 2007; Vol. 3.

(34) Glauber, R. J. Coherent and incoherent states of the radiation field. *Phys. Rev.* **1963**, *131*, 2766.

(35) Blackstock, A.; Ritchie, R.; Birkhoff, R. Mean free path for discrete electron energy losses in metallic foils. *Phys. Rev.* **1955**, *100*, 1078−1083.

(36) Pines, D. Collective energy losses in solids. *Rev. Mod. Phys.* **1956**, *28*, 184−198.

(37) Powell, C.; Swan, J. Origin of the characteristic electron energy losses in aluminum. *Phys. Rev.* **1959**, *115*, 869−875.

(38) Ghosh, R.; Mandel, L. Observation of nonclassical effects in the interference of two photons. *Phys. Rev. Lett.* **1987**, *59*, 1903−1905.

DOI: 10.1021/ph500387c
ACS Photonics 2015, 2, 157−164

(39) Kuzucu, O.; Wong, F. N.; Kurimura, S.; Tovstonog, S. Time-resolved single-photon detection by femtosecond upconversion. *Opt. Lett.* **2008**, *33*, 2257−2259.
(40) Fano, U. Quantum theory of interference effects in the mixing of light from phase-independent sources. *Am. J. Phys.* **1961**, *29*, 539−545.
(41) Ausloos, M.; Clippe, P.; Lucas, A. Infrared active modes in large clusters of spheres. *Phys. Rev. B* **1978**, *18*, 7176.
(42) Crowell, J.; Ritchie, R. Radiative decay of coulomb-stimulated plasmons in spheres. *Phys. Rev.* **1968**, *172*, 436−440.
(43) Boardman, A. D. *Electromagnetic Surface Modes*; John Wiley & Sons, 1982.
(44) Waks, E.; Sridharan, D. Cavity QED treatment of interactions between a metal nanoparticle and a dipole emitter. *Phys. Rev. A* **2010**, *82*, 043845.

DOI: 10.1021/ph500387c
ACS Photonics 2015, 2, 157−164